




## RESEARCH ARTICLE

# Sulforaphane prevents diabetes-induced hepatic ferroptosis by activating Nrf2 signaling axis

Nevena Savic<sup>1</sup>  | Milica Markelic<sup>2</sup> | Ana Stancic<sup>1</sup> | Ksenija Velickovic<sup>2</sup>  |  
 Ilijana Grigorov<sup>1</sup> | Milica Vucetic<sup>3</sup> | Vesna Martinovic<sup>1</sup> | Andjelija Gudelj<sup>1</sup> |  
 Vesna Otasevic<sup>1</sup> 

<sup>1</sup>Department of Molecular Biology, Institute for Biological Research “Siniša Stanković,” National Institute of Republic of Serbia, University of Belgrade, Belgrade, Serbia

<sup>2</sup>Department of Cell and Tissue Biology, Faculty of Biology, University of Belgrade, Belgrade, Serbia

<sup>3</sup>Medical Biology Department, Centre Scientifique de Monaco (CSM), Monaco, Monaco

## Correspondence

Vesna Otasevic, Department of Molecular Biology, Institute for Biological Research “Sinisa Stankovic,” National Institute of Republic of Serbia, University of Belgrade, Belgrade, Serbia.

Email: [vesna@ibiss.bg.ac.rs](mailto:vesna@ibiss.bg.ac.rs)

## Funding information

The Ministry of Science, Technological Development and Innovation of the Republic of Serbia, Grant/Award Number: 451-03-47/2023-01/200007; Science Fund of the Republic of Serbia, Grant/Award Number: 6525651

## Abstract

Recently, we characterized the ferroptotic phenotype in the liver of diabetic mice and revealed nuclear factor (erythroid-derived-2)-related factor 2 (Nrf2) inactivation as an integral part of hepatic injury. Here, we aim to investigate whether sulforaphane, an Nrf2 activator and antioxidant, prevents diabetes-induced hepatic ferroptosis and the mechanisms involved. Male C57BL/6 mice were divided into four groups: control (vehicle-treated), diabetic (streptozotocin-induced; 40 mg/kg, from Days 1 to 5), diabetic sulforaphane-treated (2.5 mg/kg from Days 1 to 42) and non-diabetic sulforaphane-treated group (2.5 mg/kg from Days 1 to 42). Results showed that diabetes-induced inactivation of Nrf2 and decreased expression of its downstream anti-ferroptotic molecules critical for antioxidative defense (catalase, superoxide dismutases, thioredoxin reductase), iron metabolism (ferritin heavy chain (FTH1), ferroportin 1), glutathione (GSH) synthesis (cystine-glutamate antiporter system, cystathionase, glutamate-cysteine ligase catalytic subunit, glutamate-cysteine ligase modifier subunit, glutathione synthetase), and GSH recycling - glutathione reductase (GR) were reversed/increased by sulforaphane treatment. In addition, we found that the ferroptotic phenotype in diabetic liver is associated with increased ferritinophagy and decreased FTH1 immunopositivity. The

**Abbreviations:** 4-HNE, 4-hydroxy-2-nonenal; ACC, acetyl-CoA carboxylase; ALT, alanine aminotransferase; AST, aspartate aminotransferase; CAT, catalase; CBS, cystathionine  $\beta$ -synthase; CTH, cystathionase; cystine, oxidized form of cysteine; DMT1, divalent metal transporter 1;  $Fe^{2+}$ , ferrous ion;  $Fe^{3+}$ , ferric ion; FPN1, ferroportin 1; FTH1, ferritin heavy chain; GCLC, glutamate-cysteine ligase; GCLM, glutamate-cysteine ligase modifier subunit; GPX4, glutathione peroxidase 4; GR, glutathione reductase; GSH, glutathione; GSS, glutathione synthetase; LC3, microtubule-associated protein 1A/1B-light chain 3; MnSOD, manganese-superoxide dismutase; Nrf2, nuclear factor (erythroid-derived-2)-related factor 2; pACC, phospho-acetyl-CoA carboxylase; PAS, periodic acid Schiff; pNrf2, phospho-Nrf2; SFN, sulforaphane; SOD, superoxide dismutase; STZ, streptozotocin; TFR, transferrin receptor 1; TG, triglycerides; TrxR, thioredoxin reductase; xCT, cystine-glutamate antiporter system.

This is an open access article under the terms of the [Creative Commons Attribution](https://creativecommons.org/licenses/by/4.0/) License, which permits use, distribution and reproduction in any medium, provided the original work is properly cited.

© 2024 The Authors. *BioFactors* published by Wiley Periodicals LLC on behalf of International Union of Biochemistry and Molecular Biology.

antiferroptotic effect of sulforaphane was further evidenced through the increased level of GSH, decreased accumulation of labile iron and lipid peroxides (4-hydroxy-2-nonenal, lipofuscin), decreased ferritinophagy and liver damage (decreased fibrosis, alanine aminotransferase, and aspartate aminotransferase). Finally, diabetes-induced increase in serum glucose and triglyceride level was significantly reduced by sulforaphane. Regardless of the fact that this study is limited by the use of one model of experimentally induced diabetes, the results obtained demonstrate for the first time that sulforaphane prevents diabetes-induced hepatic ferroptosis *in vivo* through the activation of Nrf2 signaling pathways. This nominates sulforaphane as a promising phyto-pharmaceutical for the prevention/alleviation of ferroptosis in diabetes-related pathologies.

#### KEYWORDS

diabetes, ferritinophagy, ferroptosis, GSH metabolism, iron metabolism, liver pathology, Nrf2, sulforaphane

## 1 | INTRODUCTION

Diabetes is a complex metabolic disorder that leads to the development of pathological changes in many organs, including liver.<sup>1,2</sup> Today, it is a well-known fact that the core of diabetic liver pathology is the loss of hepatocytes resulting from apoptosis, necrosis, autophagy, and pyroptosis.<sup>3–9</sup> In our recent study, a ferroptosis of hepatocytes in diabetic liver was discovered for the first time.<sup>10</sup> Ferroptosis is a novel, iron-dependent form of regulated cell death characterized by the accumulation of iron-induced lipid peroxides to lethal levels, resulting in oxidative damage of cells.<sup>11</sup> This type of cell death is triggered by dysfunction of the cystine-glutamate antiporter system (xCT), depletion of glutathione (GSH), and inactivation of glutathione peroxidase 4 (GPX4), a membrane associated isoform of GPX family specialized for removal of lipid peroxides. It is important to note that these core ferroptosis regulators are under the control of the transcription factor nuclear factor (erythroid-derived-2)-related factor 2 (Nrf2).<sup>12</sup> Recently, we discovered that inactivation of Nrf2, followed by an impaired axis of its downstream target proteins related to ferroptosis and involved in the metabolism of lipids, GSH, and antioxidative defense, as well as an increase in pro-oxidative, ferroptosis-related markers, is part of the ferroptotic phenotype in the liver.<sup>10</sup> Inactivated Nrf2-dependent signaling cascade was also found as an integral part of ferroptosis in diabetic models of osteoporosis,<sup>13</sup> nephropathy,<sup>14</sup> cardiomyopathy,<sup>15,16</sup> myocardial ischemia–reperfusion injury,<sup>17</sup> and pancreatic beta cells dysfunction.<sup>18</sup> All of the above highlights the critical importance of ferroptosis in the pathogenesis of diabetes

and its comorbidities, and suggests activation of the Nrf2-dependent cascade as a potential therapeutic approach to suppress ferroptosis.

By virtue of its lipophilic nature, sulforaphane (SFN; 1-isothiocyanato-4-[methylsulfinyl] butane), a natural sulfur-rich compound found in cruciferous vegetables, has emerged as a powerful Nrf2 activator.<sup>19,20</sup> Compared with widely used phytochemical supplements (such as curcumin, silymarin, and resveratrol), SFN exhibits significantly higher bioavailability and more potent activation of Nrf2 and its downstream cytoprotective genes.<sup>20</sup> SFN exerts a wide range of biological effects, such as anti-oxidative, anti-inflammatory, anticancer, antimicrobial activity, and so on.<sup>21,22</sup> In diabetic pathology, SFN has been recognized as a powerful agent for reducing hyperglycemia and hyperlipidemia, improving insulin resistance, diabetes-induced oxidative stress and inflammation,<sup>23–26</sup> and preventing the development of diabetic cardiomyopathy, nephropathy, neuropathy, retinopathy, and liver damage.<sup>19,26,27</sup> These antidiabetic effects and especially the fact that SFN is a very potent natural Nrf2 activator make it an excellent candidate for testing antiferroptotic potential in the diabetic liver. Its antiferroptotic effect on the liver has been found in models of acute liver injury<sup>28</sup> and nonalcoholic fatty liver disease,<sup>29</sup> but beyond that, the protective effects of SFN, particularly in the context of diabetes, have not been studied. Therefore, this study aimed to investigate whether SFN can ameliorate diabetes-induced hepatic ferroptosis, that is, liver damage by activating the Nrf2-signaling pathway, with special emphasis to the antiferroptotic effect of SFN through iron and GSH metabolism.

## 2 | RESULTS

The results obtained here are from an experimental setup with four experimental groups which include diabetic untreated mice (DM), diabetic mice treated with SFN (DM + SFN), a group of non-diabetic mice treated with SFN only (SFN) to test the effect of the substance itself, and an untreated control mice (Ctrl). Diabetes was induced in both groups with five low doses of STZ, from Days 1 to 5, while SFN was administered on 1–42 days of the experiment. The applied doses of STZ and SFN are given in Section 2.1.

### 2.1 | Sulforaphane treatment activated Nrf2 in hepatocytes of diabetic mice

Immunohistochemical detection of total Nrf2 (Figure 1A) showed its decreased presence in the liver of diabetic (DM) mice, primarily observed in hepatocytes of the centrolobular regions, as well as a reduction in Nrf2 nuclear translocation (Figure 1B) when compared to the control group ( $p < 0.05$ ). Treatment of the diabetic animals with SFN enhanced Nrf2 nuclear translocation toward the

control level. This was consistent with data obtained by WB analysis which revealed a significant decrease in pNrf2, the activated, nuclear form of Nrf2 (Figure 1D) in the DM group compared to the control group ( $p < 0.001$ ), while SFN treatment of DM mice restored pNrf2 to the control level and significantly increased it compared to the DM group ( $p < 0.001$ ). No alternations of total Nrf2 were found by WB analysis in any of the examined groups (Figure 1C).

### 2.2 | Sulforaphane attenuates pro-oxidative ferroptotic parameters and improves antioxidative defense in the liver of diabetic mice

Taking into account the fact that iron-induced lipid peroxidation is a central event in the process of ferroptosis, markers of lipid peroxidation, 4-HNE and lipofuscin were analyzed. Immunohistochemical detection of 4-HNE is presented in Figure 2A. Quantification of immunohistochemical detection of 4-HNE in liver tissue (Figure 2C) revealed a significant increase in immunopositivity of liver cells in diabetic animals ( $p < 0.001$ ). The presence

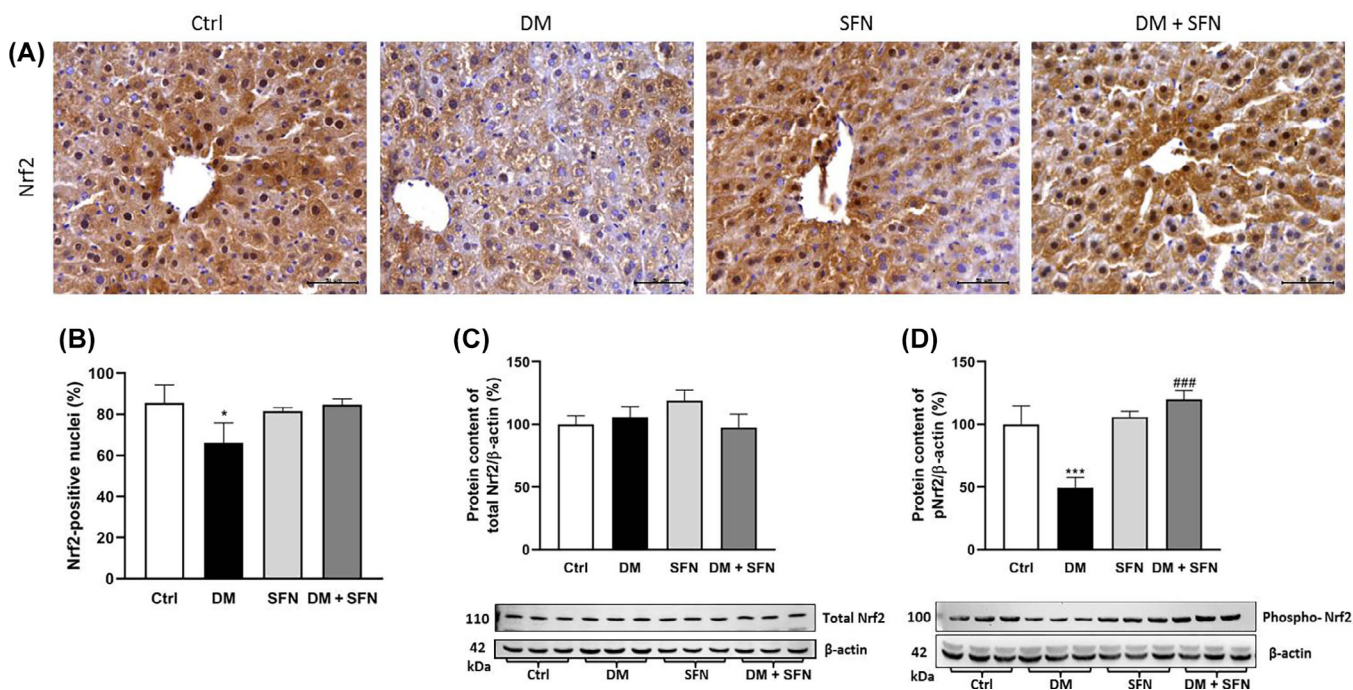


**FIGURE 1** Nrf2 Protein content and its activation status in liver tissue of control (Ctrl), diabetic (DM), non-diabetic SFN-treated (SFN) and diabetic SFN-treated mice (DM + SFN). (A) Representative micrographs of Nrf2 immunohistochemical detection ( $n = 3$  animals per group); scale bars: 50 μm; and (B) quantification of Nrf2 nuclear immunopositivity expressed as percentage ratio of positive nuclei to total number of nuclei surrounding central veins. Protein content of (C) total Nrf2 and (D) phosphorylated Nrf2 form (pNrf2)—β-actin serves as protein loading control for both blots. Values are expressed relative to the non-diabetic control group which was standardized to 100% ( $n = 8$ , each band represents pooled samples). Values are presented as means  $\pm$  SD. Statistical significance: Comparison to Ctrl group (\*),  $*p < 0.05$  and  $***p < 0.001$ ; DM versus DM + SFN comparison (#),  $###p < 0.001$ .

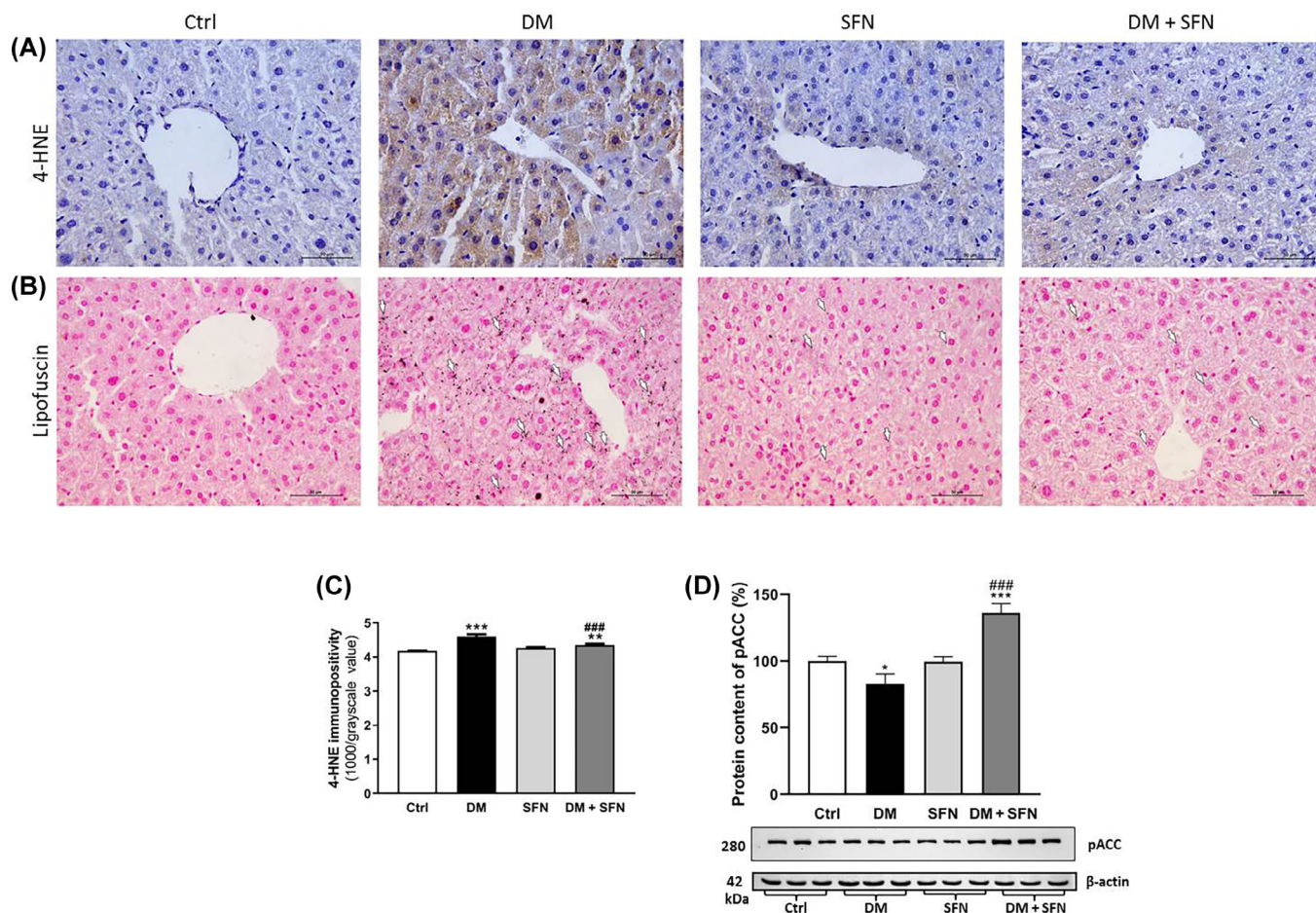


**FIGURE 2** Lipid peroxidation-related parameters in liver tissue of control (Ctrl), diabetic (DM), non-diabetic SFN-treated (SFN), and diabetic SFN-treated mice (DM + SFN). (A) Representative micrographs of immunohistochemical detection of 4-HNE ( $n = 3$  animals per group); scale bars: 50  $\mu$ m and (C) quantification of 4-HNE tissue immunopositivity. (B) Representative micrographs of lipofuscin detection by Sudan Black B staining, arrows point to black-stained lipofuscin particles inside hepatocytes (h); scale bars: 50  $\mu$ m. (D) Protein content of phosphorylated ACC form (pACC)— $\beta$ -actin serves as protein loading control. Values are expressed relative to the non-diabetic control group which was standardized to 100% ( $n = 8$ , each band represents pooled samples). Values are presented as means  $\pm$  SD. Statistical significance: Comparison to Ctrl group (\*), \* $p < 0.05$ , \*\* $p < 0.01$ , and \*\*\* $p < 0.001$ ; DM versus DM + SFN comparison (#), ### $p < 0.001$ .

of 4-HNE adducts significantly declined toward control levels when diabetic animals were treated with SFN, and a significant reduction was seen when compared to the DM group ( $p < 0.001$ ). No significant alterations in the hepatic 4-HNE immunopositivity level were noted in the SFN-treated non-diabetic animals. Microscopic observation of lipofuscin (Figure 2B) showed its higher accumulation in the hepatocytes of diabetic mice related to the control. In accordance with lower 4-HNE presence, SFN treatment of diabetic mice decreased lipofuscin accumulation.

Next, in order to detect eventual alternations in the biosynthesis of fatty acids, including PUFAs—the main substrate for the initiation of lipid peroxidation, expression of inactivated acetyl-CoA carboxylase form - pACC was analyzed (Figure 2D). Our results showed significant

decrease of this enzyme in the DM mice compared to the control ( $p < 0.05$ ), while SFN treatment of diabetic mice led to a markedly increased level of pACC in comparison with both control and diabetic mice ( $p < 0.001$  for both).

Regarding antioxidative defense enzymes, a significant decrease in the activity of total SOD (Figure 3A) and its mitochondrial isoform MnSOD (Figure 3B) ( $p < 0.05$  and  $p < 0.01$ , respectively), as well as the protein levels of CAT (Figure 3C) and TrxR (Figure 3D) were detected in the liver of DM mice ( $p < 0.001$  and  $p < 0.05$ , respectively). SFN treatment of diabetic mice completely restored MnSOD activity to the control level and significantly increased the protein level of CAT when compared to DM group ( $p < 0.01$ ). All of the examined parameters of antioxidative defense remained unaltered in the liver of SFN-treated non-diabetic mice.

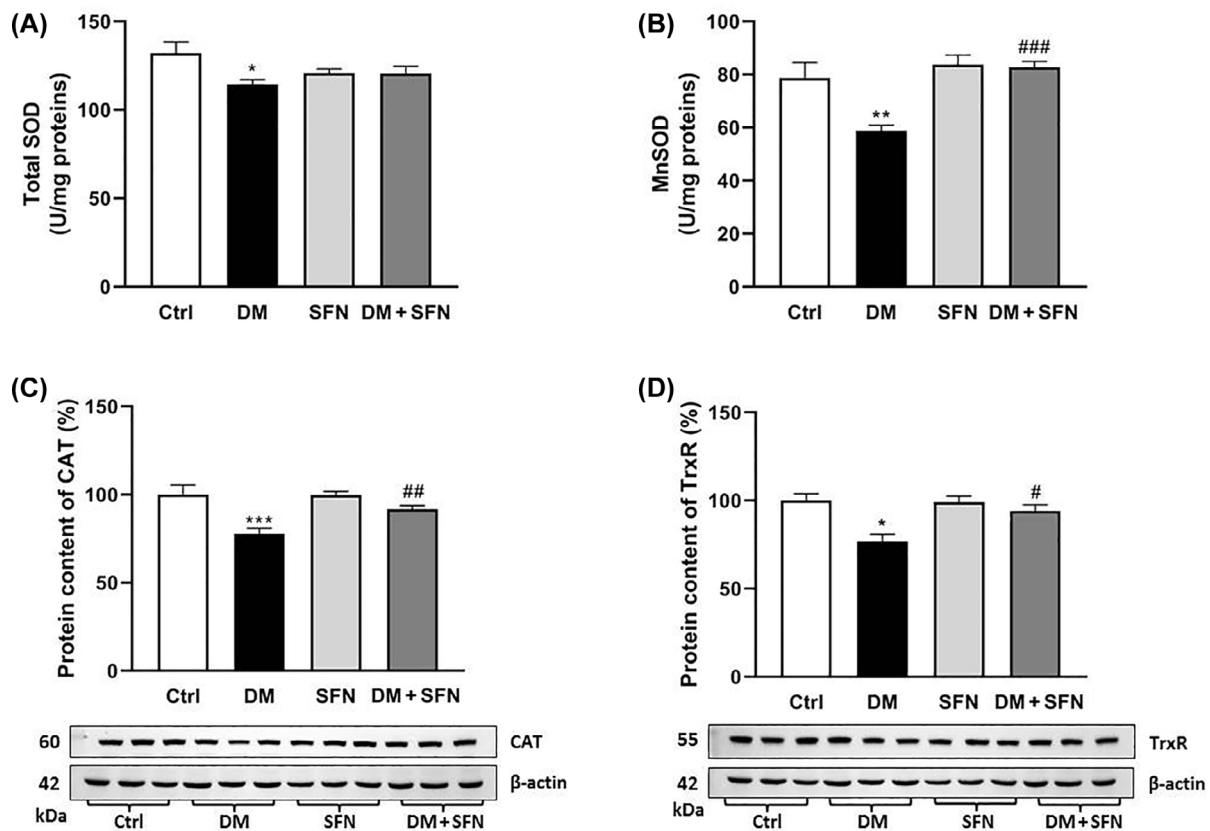


**FIGURE 3** Parameters of antioxidative defense in liver tissue of control (Ctrl), diabetic (DM), non-diabetic SFN-treated (SFN), and diabetic SFN-treated mice (DM + SFN). Enzyme activity of (A) total SOD and (B) MnSOD ( $n = 8$  animals per group). Protein content of (C) CAT and (D) TrxR— $\beta$ -actin serves as protein-loading control for both blots. Values are expressed relative to the non-diabetic control group which was standardized to 100% ( $n = 8$ , each band represents pooled samples). Values are presented as means  $\pm$  SD. Statistical significance: Comparison to Ctrl group (\*),  $*p < 0.05$ ,  $**p < 0.01$ , and  $***p < 0.001$ ; DM versus DM + SFN comparison (#),  $\#p < 0.05$ ,  $##p < 0.01$ , and  $###p < 0.001$ .

### 2.3 | Effects of sulforaphane on iron metabolism and ferritinophagy in hepatocytes

In order to examine changes in iron metabolism in diabetic liver, the tissue iron loading and the expression of the main proteins that regulate labile iron pool were analyzed. Histochemical detection of iron ( $\text{Fe}^{3+}$ ) in the liver revealed its increased accumulation in hepatocytes of diabetic animals when compared to control animals in which rare, individual iron-loaded cells are detectable (Figure 4A). In addition to many hepatocytes, some endothelial cells of hepatic veins of diabetic animals are also iron-loaded. SFN reduced intracellular free iron accumulation to the control level in diabetic animals, while in non-diabetic animals iron level remained unaltered.

Immunohistochemical analysis of DMT1 (Figure 4B) showed increased immunopositivity of DMT1 in hepatocytes and endothelial cells of the diabetic mice, while SFN treatment slightly attenuated DMT1 hepatic

immunopositivity, restoring it toward the control level. Additionally, the protein content of FTH1 (Figure 4C) and FPN1 (Figure 4D), was significantly decreased in the liver of DM mice, compared to the control group ( $p < 0.001$ , for both). SFN treatment of diabetic animals resulted in increased expression of FTH1 and FPN1 ( $p < 0.001$ , for both) compared to the diabetic group, and in the case of FPN1, even above the control level ( $p < 0.001$ ). Treatment of non-diabetic control animals with SFN resulted in a significant increase in FPN1 level compared to control ( $p < 0.05$ ).

Furthermore, to examine if the decrease of FTH1 protein level in the liver of DM mice is accompanied by its autophagy (i.e., ferritinophagy), double immunofluorescence detection of FTH1 and autophagosome-related protein LC3 was performed. As shown in Figure 5A, homogenous FTH1 immunopositivity is detectable in liver tissue of control group, including both hepatocytes and endothelial cells, while LC3 is detectable primarily in some hepatocytes, mostly surrounding centroportal

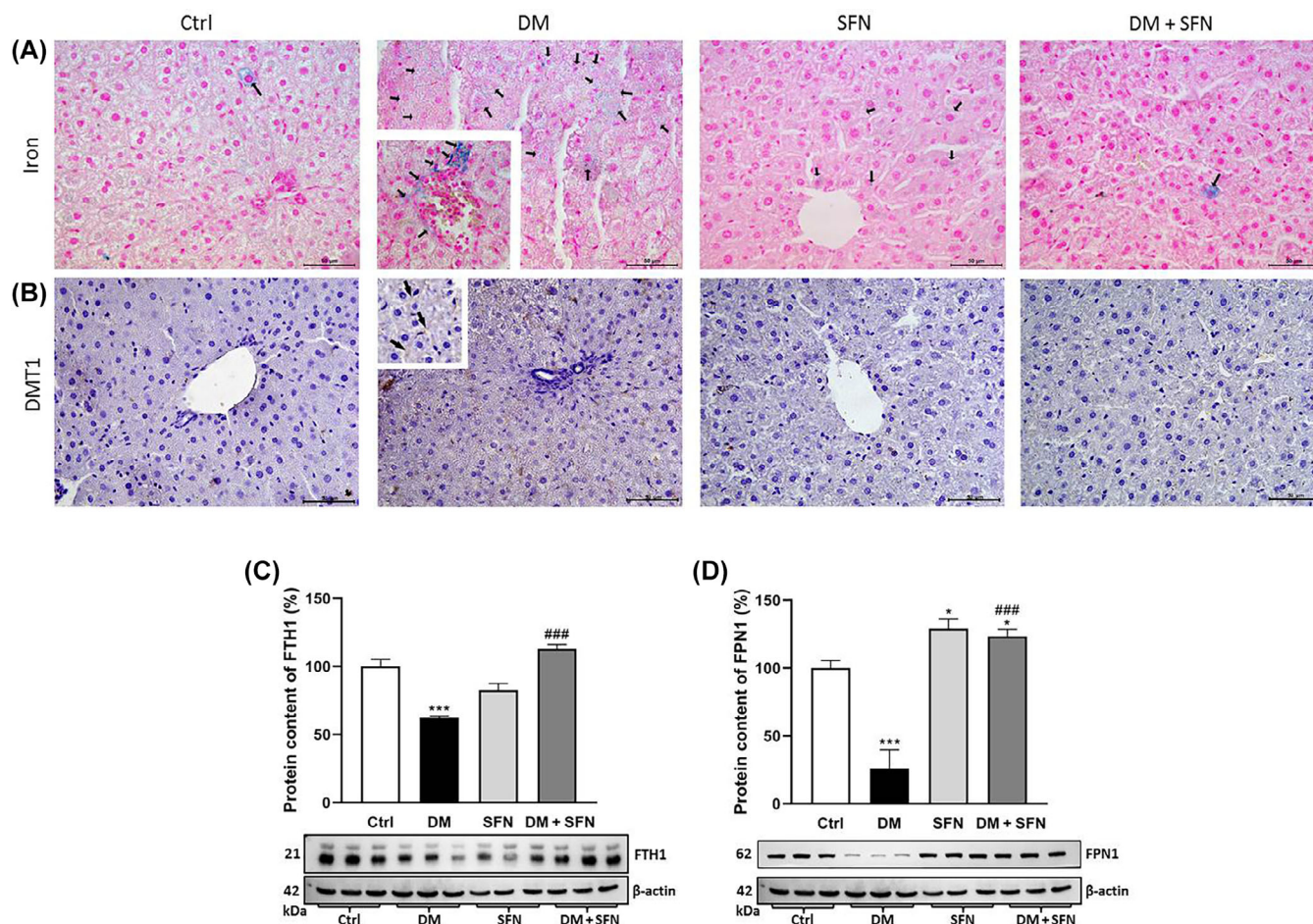


**FIGURE 4** Tissue iron load and the content of proteins related to iron metabolism in liver tissue of (Ctrl), diabetic (DM), non-diabetic SFN-treated (SFN), and diabetic SFN-treated mice (DM + SFN). Representative micrographs of (A) Prussian blue detection of  $\text{Fe}^{3+}$ , indicated by black arrows; scale bars: 50  $\mu\text{m}$ , and of (B) immunohistochemical detection of DMT1; scale bars: 50  $\mu\text{m}$  ( $n = 3$  animals per group); examination of protein content of (C) FTH1 and (D) FPN1— $\beta$ -actin serves as protein-loading control for both blots. Values are expressed relative to the non-diabetic control group which was standardized to 100% ( $n = 8$ , each band represents pooled samples). Values are presented as means  $\pm$  SD. Statistical significance: Comparison to Ctrl group (\*),  $*p < 0.05$  and  $***p < 0.001$ ; DM versus DM + SFN comparison (#),  $###p < 0.001$ .

vein. Although hepatocyte FTH1 immunopositivity decreases in diabetic liver, remaining high in the endothelial cells of sinusoids, the colocalization rate of FTH1 with LC3 in hepatocytes (Figure 5B) of DM mice was significantly higher in comparison to the control values ( $p < 0.05$ ). SFN treatment of DM mice returned the colocalization rate of these proteins inside hepatocytes to control level ( $p < 0.05$  compared to DM group).

## 2.4 | Sulforaphane improved GSH metabolism in the liver of diabetic mice

Initially, we were interested in investigating whether and how GSH level changed with the treatments. As expected, a significantly decreased level of GSH was seen

in the liver of DM mice compared to the control ( $p < 0.001$ ) (Figure 6C). SFN treatment of diabetic animals restored GSH level and significantly increased it compared to DM mice ( $p < 0.01$ ). In non-diabetic group treated with SFN, GSH level stayed unaltered compared to the control.

Next, we examined the possible changes in protein expression of key enzymes responsible for GSH synthesis/recycling/consumption in the liver. The changes in the levels of proteins involved in the *de novo* synthesis of cysteine, CBS and CTH, and in cystine import (xCT antiporter), which limit GSH synthesis, are shown in Figure 6A. A markedly decreased level of CTH was found in the liver of the diabetic mice ( $p < 0.001$ ), while the protein content of CBS remained at the control level. SFN treatment of the diabetic mice significantly

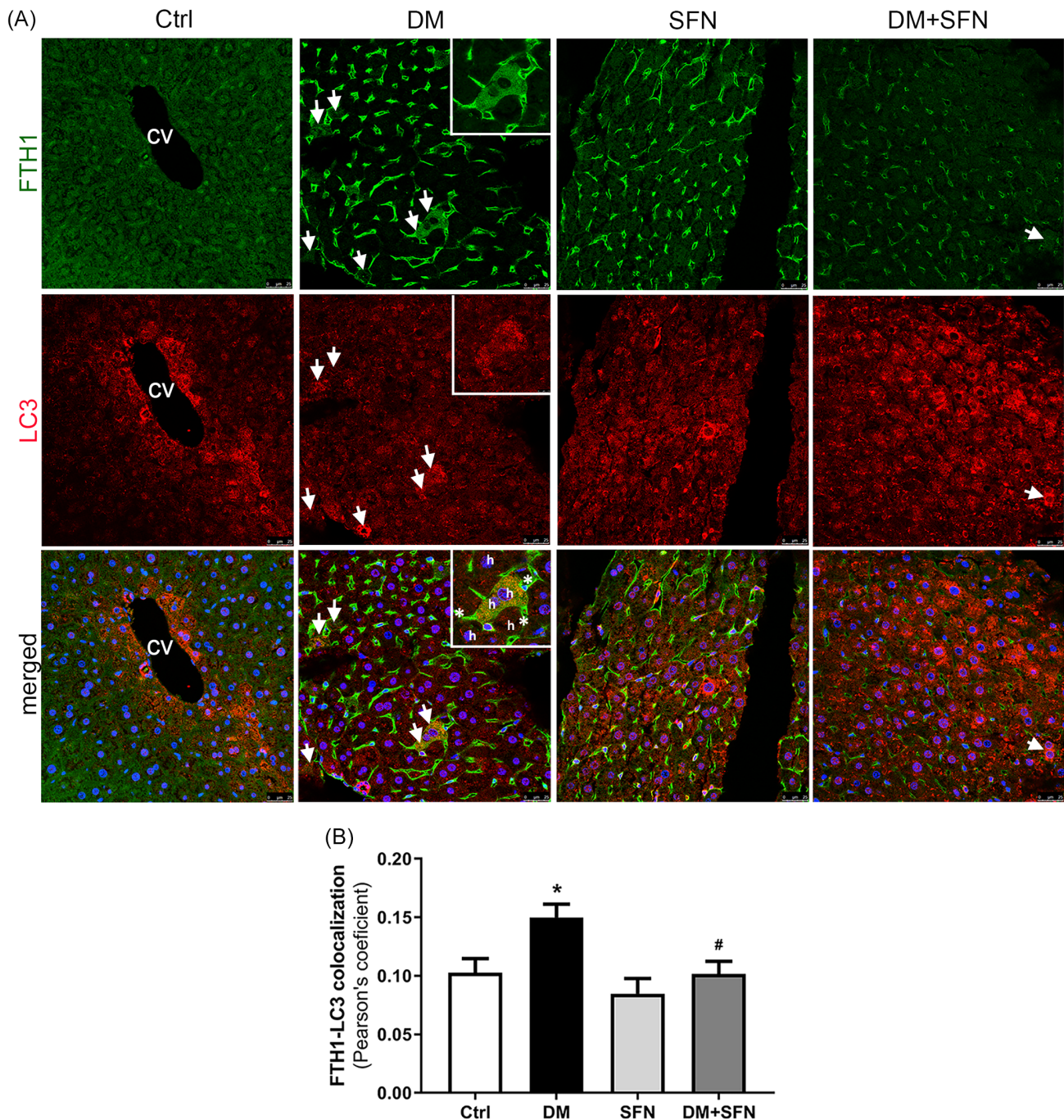


**FIGURE 5** Colocalization of FTH1 and LC3 in liver of control (Ctrl), diabetic (DM), non-diabetic SFN-treated (SFN) and diabetic SFN-treated mice (DM + SFN). (A) Double immunofluorescence detection of: FTH1 (green signal), LC3 (red signal) and superimposed signals from FTH1, LC3 and nuclei (blue); cv, central vein; white arrows, hepatocytes with higher rate of colocalization of FTH1 and LC3; insets, representative hepatocytes (h) with strong colocalization of FTH1 and LC3, surrounded by the FTH1-positive endothelial cells (\*) of sinusoids. Scale bars: 25  $\mu\text{m}$  ( $n = 3$  animals per group). (B) Quantification of FTH1-LC3 colocalization rate presented as mean Pearson coefficient. Values are presented as means  $\pm$  SD. Statistical significance: comparison to Ctrl group (\*),  $*p < 0.05$ ; DM versus DM + SFN comparison (#),  $\#p < 0.05$ .

increased protein level of CTH and CBS compared to the DM group ( $p < 0.001$  and  $p < 0.05$ , respectively), and increased CBS level even above the control level ( $p < 0.01$ ). Similarly, in non-diabetic animals, SFN

increased the level of CTH and CBS above the control level ( $p < 0.05$  and  $p < 0.01$ , respectively). Examination of xCT protein content revealed a significant decrease in the liver of DM mice, compared to the control

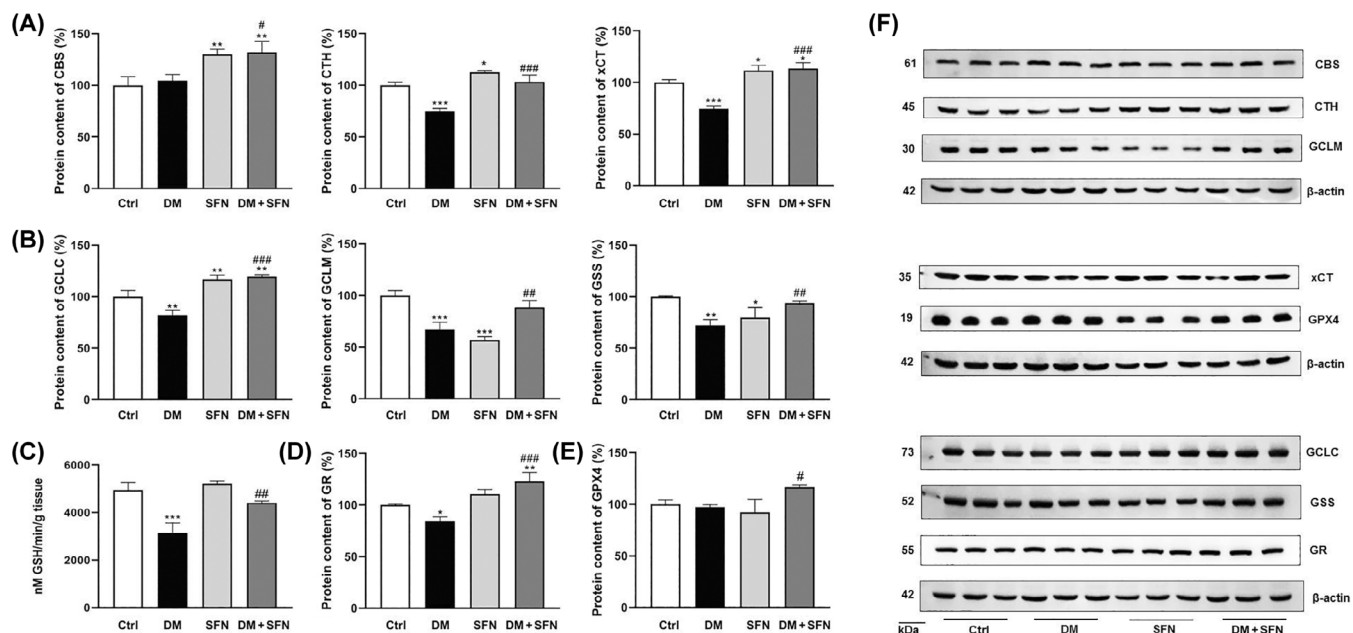


**FIGURE 6** GSH and proteins involved in GSH metabolism in liver tissue of control (Ctrl), diabetic (DM), non-diabetic SFN-treated (SFN), and diabetic SFN-treated mice (DM + SFN). (C) GSH amount and content of proteins involved in: (A) cysteine synthesis—CBS, CTH, and cystine transport—xCT, (B) GSH synthesis—GCLC, GCLM and GSS, as well as (D) in recycling of reduced GSH—GR. (E) Protein content of GPX4. (F) Representative blots with corresponding protein-loading controls ( $\beta$ -actin). Values are expressed relative to the non-diabetic control which was standardized to 100% ( $n = 8$ , each band represents pooled samples). Values are presented as means  $\pm$  SD. Statistical significance: Compared to Ctrl group (\*), \* $p < 0.05$ , \*\* $p < 0.01$ , and \*\*\* $p < 0.001$ ; DM versus DM + SFN comparison (#), # $p < 0.05$ , ## $p < 0.01$ , and ### $p < 0.001$ .

( $p < 0.001$ ). SFN significantly increased xCT protein content above control level in both diabetic and non-diabetic animals ( $p < 0.05$  for both), as well as in diabetic animals compared to the diabetic untreated group ( $p < 0.001$ ).

Furthermore, the levels of proteins involved in GSH synthesis, that is, both subunits of glutamate-cysteine ligase—catalytic (GCLC) and regulatory (GCLM), as well as GSS, were investigated (Figure 6B). Compared to the control, diabetes significantly decreased protein expression of GCLC, GCLM, and GSS in the liver of mice ( $p < 0.01$ ,  $p < 0.001$ , and  $p < 0.01$  respectively), while SFN treatment of diabetic mice significantly increased the level of all examined proteins compared to DM ( $p < 0.001$ ,  $p < 0.01$ ,  $p < 0.01$ , respectively) and even above the control value in the case of GCLC ( $p < 0.01$ ). Unlike GCLC and GSS, whose level in the SFN-treated non-diabetic group stayed unaltered compared to the control, the content of GCLM was significantly lower ( $p < 0.001$ ).

In addition, the protein level of GR (Figure 6D), which is involved in the recycling pathway of reduced GSH, was significantly decreased in the livers of the diabetic animals compared to the control ( $p < 0.05$ ). However, SFN treatment of the diabetic animals restored the control level of GR ( $p < 0.001$ , in comparison to the DM group) and even increase it above control value

( $p < 0.01$ ). Finally, the analysis of GPX4 (Figure 6E), showed that SFN treatment of the DM animals significantly increased the protein level of GPX4 compared to the DM group ( $p < 0.05$ ), while in the DM group, as well as in SFN group, the GPX4 level remained unchanged compared to the control mice.

## 2.5 | Beneficial effects of sulforaphane on physical, biochemical, and histomorphological parameters in diabetic animals

Our results show that SFN contributes to the overall improvement of diabetic condition in mice by normalizing glycemia, insulin level, body mass, and liver function itself. Namely, serum glucose levels (Figure 7A) increased significantly in the DM group compared to the control, as early as Day 14 of the experiment ( $p < 0.001$ ). From this point on, glycemia in the DM group remained significantly elevated ( $p < 0.001$ ) until the end of the experiment. Despite the initial increase in glycemia in the DM + SFN group ( $p < 0.001$ ) at Day 14, a decrease in blood glucose levels toward control levels was observed from this point onward with SFN treatment, and a significant decrease compared to the untreated diabetic group was



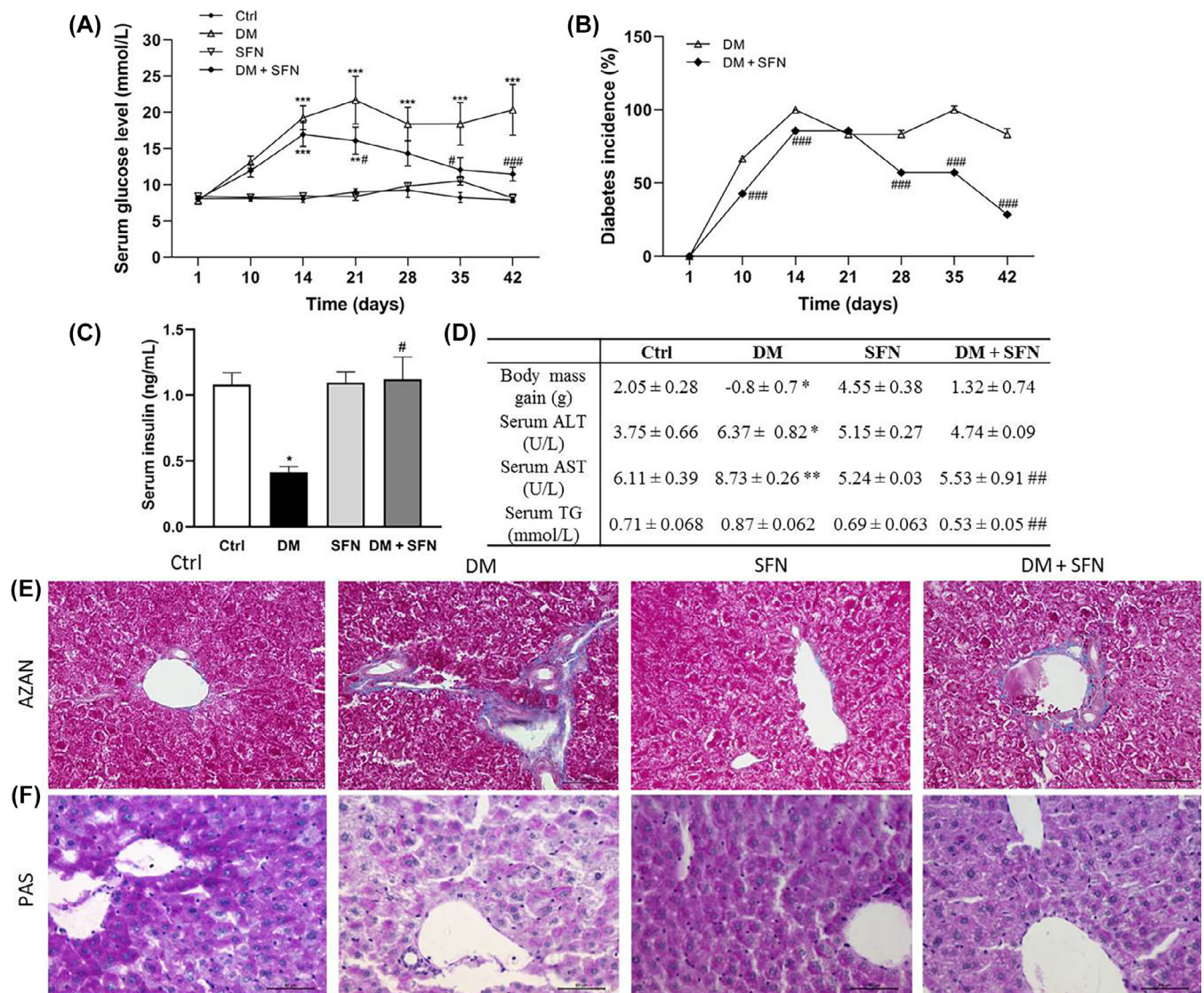


**FIGURE 7** Physical and biochemical characteristics of experimental groups and histopathological analysis of liver tissue from control (Ctrl), diabetic (DM), non-diabetic SFN-treated (SFN), and diabetic SFN-treated mice (DM + SFN). (A) Serum glucose levels and (B) diabetes incidence in the DM and DM + SFN groups; both were measured at different time points of the experiment (1, 10, 14, 21, 28, 35, and 42 days);  $n = 8$ . (C) Serum insulin level;  $n = 8$ . (D) Body mass gain (difference in body mass between the last and first day of the experiment) and serum hepatogram parameters (ALT, AST, and TG);  $n = 8$ . Microscopic detection of (E) liver fibrosis by AZAN staining of collagen fibers (\*) surrounding blood vessels and of (F) glycogen inside hepatocytes (red) by PAS staining; scale bars for both stainings: 50  $\mu\text{m}$  ( $n = 3$  animals per group). Values are given as means  $\pm$  SEM. Statistical significance: comparison to Ctrl group (\*),  $*p < 0.05$ ,  $**p < 0.01$  and  $***p < 0.001$ ; DM versus DM + SFN comparison (#),  $\#p < 0.05$ ,  $##p < 0.01$ ,  $###p < 0.001$ .

achieved on Days 21, 35, and 42 ( $p < 0.05$ ,  $p < 0.05$ , and  $p < 0.001$ , respectively). In the non-diabetic SFN-treated group, glycemia remained at the control level throughout the experiment. The incidence of diabetes (Figure 7B), calculated as the percentage of hyperglycemic animals, showed that the incidence in the DM group reached a value above 50% already on the 10th day of the experiment and gradually increased above this value over time. In the diabetic mice SFN significantly reduced the incidence of diabetes at Days 10, 14, 28, 35, and 42 ( $p < 0.001$  for all time points), compared with DM

mice. Measurement of serum insulin levels (Figure 7C) showed that insulin levels had significantly decreased in DM mice compared with the control group ( $p < 0.05$ ), while SFN treatment of DM mice restored insulin levels to control values ( $p < 0.05$  compared with the DM group).

As seen in Figure 7D body mass gain was significantly reduced in the DM mice compared to the control mice ( $p < 0.05$ ), while body mass gain remained at the control level in both diabetic and non-diabetic groups treated with SFN. In addition, our results indicate that SFN

reduces diabetes-induced liver damage, as evidenced by the restoration of hepatogram parameters to homeostatic levels. Namely, ALT and AST levels (Figure 7D) were significantly higher in the DM group compared to the control group ( $p < 0.05$  and  $p < 0.01$ , respectively), while treatment of diabetic animals with SFN restored the control levels of both AST and ALT and significantly reduced the level of AST compared to DM ( $p < 0.01$ ). Serum TG level (Figure 7D) was slightly elevated in the DM group, but without significance, while significantly decreased in the DM + SFN group compared to the DM group ( $p < 0.01$ ). There were no significant alterations in ALT, AST, and TG levels in the non-diabetic SFN-treated group compared to the control.

To determine histopathological alterations in the liver, AZAN trichrome and PAS staining were performed. Masson's AZAN trichrome-staining clearly shows increased fibrosis in the liver of the diabetic mice, as evidenced by increased accumulation of blue-stained collagen fibers around the blood vessels (Figure 7E). In the diabetic group treated with SFN, fibrosis decreased and the overall morphological appearance of the liver improved. Glycogen detection by PAS staining (Figure 7F) revealed that diabetes resulted in a marked decrease in red-stained glycogen depots in the liver. On the other hand, glycogen content was visibly less reduced in SFN-treated diabetic animals. No histopathological changes regarding fibrosis induction or glycogen depletion were noted in the liver of SFN-treated non-diabetic animals.

### 3 | DISCUSSION

In this study, we showed that SFN exerts a significant anti-ferroptotic potential in the liver of diabetic mice. This beneficial effect of SFN is achieved through the activation of Nrf2 and its downstream anti-ferroptotic pathways, particularly those related to GSH and iron metabolism.

The biological activity of SFN and its protective effects are realized by stimulating the antioxidative and anti-inflammatory response, mainly through the activation of the signaling cascade of Nrf2 transcription factor.<sup>30,31</sup> It is well known that SFN activates Nrf2, directly via kinase-dependent phosphorylation or indirectly through inhibiting Nrf2 ubiquitination, thereby enabling its further phosphorylation.<sup>19,32</sup> Since our results have shown no alternations in total Nrf2 form it can be concluded that here, a beneficial effect of SFN on diabetic liver is achieved by enhancing Nrf2 activation, indicated by an increased level of pNrf2 and reinforced nuclear translocation of this transcription factor. The similar effect on Nrf2 activation was observed under

physiological conditions in non-diabetic mice treated with SFN. These results are in agreement with the numerous data reporting increased Nrf2 activation by SFN treatment.<sup>33–35</sup>

In the nucleus, Nrf2 can directly activate the expression of genes that primarily regulate the antioxidant defense and detoxification of the cell.<sup>31,36</sup> In this context, we investigated changes in labile iron pool, and the read-outs of secondary lipid peroxidation products—4-HNE and lipofuscin, since iron-induced lipid peroxidation is a specific trigger of ferroptosis.<sup>37</sup> The obtained results indicate beneficial effects of SFN-induced Nrf2 activation, since strong diminishment of the prooxidative phenotype was seen in the liver of diabetic mice treated with SFN. Namely, the diabetes-induced increase in iron accumulation, followed by the increased accumulation of 4-HNE and lipofuscin, was reversed by SFN treatment. Furthermore, our results suggest that SFN may prevent lipid peroxidation by reducing the synthesis of fatty acids, including PUFAs—the main substrate for the initiation of lipid peroxidation. This is evidenced by the SFN-induced inactivation of ACC, that is, its increased phosphorylation in diabetic liver. Our results are consistent with the previously described effects of SFN on reducing lipid peroxidation in the liver of mice with alcohol-induced hepatic steatosis,<sup>38</sup> and in various experimental models.<sup>25,39,40</sup>

In addition to the above-mentioned suppression of pro-oxidative ferroptotic parameters, it was observed that SFN-induced Nrf2 activation was associated with an enhancement of the antioxidative defense in the liver of diabetic mice. As shown here, SFN diminished the diabetes-induced decrease in the activity of total SOD and MnSOD, and in the protein content of CAT, that is, it strengthened the antioxidative capacity of tissue which eventually led to a decrease in prooxidant markers in diabetic liver, as shown above. The antioxidative defense proteins studied here are regulated by the binding of Nrf2 to the antioxidative response elements (ARE) in the promoter of their genes,<sup>12,41–44</sup> and their upregulation has been repeatedly confirmed by the usage of various Nrf2 activators,<sup>45,46</sup> including SFN itself.<sup>17,25,31,35,47</sup> Moreover, the observed effect of SFN on boosting antioxidative defense, thereby reducing pro-oxidative ferroptotic events in the liver of diabetic mice is consistent with the effect of the specific inhibitor of ferroptosis, ferrostatin-1, which exerted similar reduction of pro-ferroptotic parameters and liver injury in our previous study on the same diabetic model as used here.<sup>10</sup> This strongly supports the anti-ferroptotic action of SFN.

Furthermore, Nrf2 has been shown to regulate the majority of proteins involved in iron metabolism.<sup>12,15,17,48–50</sup> Therefore, we examined whether

activation of Nrf2 by SFN is followed by the corresponding changes in expression of the iron-regulating proteins. Iron content in the cell is controlled at the several levels: import of ferric ion ( $\text{Fe}^{3+}$ ) by transferrin (TFR)-induced endosomal internalization; transfer of ferrous ion ( $\text{Fe}^{2+}$ ) from the endosome to the cytosol by DMT1; storage of  $\text{Fe}^{2+}$  in the cell by binding to FTH1, and finally export of excess iron, through the transmembrane receptor FPN1.<sup>51</sup> Here, we have demonstrated that along with the inactivation of Nrf2, expression of FTH1 and FPN1 is decreased in the diabetic group, clearly indicating that markedly decreased capacity for iron storage and excretion contribute significantly to the increased accumulation of iron in the liver of diabetic mice. These data demonstrate impaired Nrf2-regulated iron homeostasis during diabetes-induced liver ferroptosis and are consistent with the data of Zhao and coworkers,<sup>52</sup> who observed downregulated FTH1 and FPN1, as part of ferroptotic phenotype in a model of ethanol-induced liver injury. In contrast, SFN apparently restored the ability of the diabetic liver to sequester and export iron by reducing diabetes-induced decreases in FPN1 and FTH1 protein levels, that is consistent with the previously described anti-ferroptotic effects of SFN observed in a diabetic models of cardiomyopathy<sup>15</sup> and myocardial ischemia–reperfusion injury.<sup>17</sup>

Moreover, our results suggest an additional effect of SFN on iron metabolism, which is achieved through Nrf2-dependent regulation of selective autophagy, that is, ferritinophagy in diabetic liver. Numerous key autophagy proteins have been shown to be regulated by Nrf2 and various Nrf2 activators have been shown to promote the expression of autophagy markers, such as LC3.<sup>53,54</sup> Our results show for the first time that SFN ameliorates diabetes-induced ferritinophagy, which was observed here by increased colocalization of FTH1 and LC3 in the liver of diabetic mice. Ferritinophagy leads to the release of iron from degraded FTH1 into the cytosol and has recently been shown to be very important for the induction and execution of ferroptosis.<sup>55,56</sup> Thus, inhibition of ferritinophagy emerged recently as a new potent strategy for inhibition of ferroptosis, and our present data strongly contribute to this issue proposing SFN as potent suppressor of ferritinophagy under diabetic conditions. In addition, SFN has been reported to be involved in various intracellular signal transductions, independent of the Nrf2 pathway.<sup>57,58</sup> Accordingly, although DMT1 is not under direct Nrf2 regulation, we have shown here that SFN decreased its immunoprecipitation in diabetic liver. Increased DMT1 expression under diabetic conditions is in accordance with increased labile iron level that we observed here, as DMT1 stimulates iron transfer from endosomes to cytosol. Thus, reducing DMT1 expression

could be one of the mechanisms involved in SFN dependent decrease of ferroptosis in diabetes, by reduction of labile iron pool in these cells. In view of the above, it can be concluded that SFN modulates cellular iron homeostasis at different levels: (i) it enhances the binding and excretion of excess free iron and (ii) it decreases iron uptake from endosomes, thereby reducing iron accumulation in the diabetic liver, and suppressing iron-induced lipid peroxidation and ferroptosis.

Furthermore, SFN significantly affects the amount of GSH in hepatocytes of diabetic liver through Nrf2-dependent regulation of key proteins responsible for regulation of GSH metabolism. Maintenance of homeostatic GSH levels through fine regulation of its metabolism is of vital importance for the cell since GSH acts as a direct scavenger of electrophiles and oxidative species, while its important role as a cofactor of GSH-related antioxidative enzymes, especially GPX4, puts it in a ferroptotic context.<sup>59</sup> Therefore, perturbations of GSH metabolism leading to GSH depletion are strongly associated with ferroptotic outcome. The amount of GSH is determined by the availability of cysteine in the cell, which is determined by its *de novo* synthesis and the uptake of its oxidized form (cystine) via xCT exchanger.<sup>60</sup> The xCT system is considered crucial for ferroptosis regulation, as cystine import by xCT represents a rate-limiting step in GSH biosynthesis.<sup>61</sup> Our results suggest that SFN improves *de novo* synthesis of cysteine based on increased expression of CBS and CTH, as well as enhanced capacity for influx of cystine, evidenced as increased xCT protein level in diabetic liver treated by SFN. In addition, SFN increases GSH level in diabetic liver by increasing expression of the enzymes involved in its synthesis, including the catalytic and modifier units of the first and limiting enzyme of GSH synthesis, GCL (GCLC and GCLM), as well as GSS. Finally, our results suggest that SFN enhances the recycling pathway of reduced GSH by increasing the expression of GR and TrxR. Since all of the aforementioned proteins are under Nrf2 transcriptional regulation,<sup>12,62–64</sup> this suggests that SFN ameliorates the disturbed synthesis and recycling pathway of GSH in diabetes, by activating the Nrf2-dependent axis, thus resulting in the overall increase of GSH amount in diabetic liver. This is consistent with the studies that have already shown that the beneficial effect of SFN on GSH metabolism is associated with increased expression of the above-mentioned proteins.<sup>25,34,38,65</sup>

In addition, we have shown that SFN increases GPX4 protein content in diabetic liver, which, together with increased GSH level and reduced accumulation of lipid peroxides, demonstrated above, undoubtedly confirmed improvement of GPX4-mediated removal of lipid peroxides by SFN. However, protein expression of GPX4 in the

diabetic group remained at the control level. This could be explained as a defense mechanism of the cells aimed at overcoming the reduced capacity of GPX4 to remove lipid peroxides under diabetic conditions, which is obviously characterized by disturbances in GSH metabolism, especially by reduced availability of its cofactor, GSH. Accordingly, a recent paper by Ursini et al.<sup>66</sup> points out to the compensatory increase in protein content of GPX4, due to the lack of GSH. It is also worth noting that ferroptosis phenotype is characterized by an obligatory accumulation of lipid peroxides, achieved either by depletion of GSH and/or a decrease of GPX4 activity/content.<sup>67</sup> All this suggests that impairment of Nrf2-dependent GSH metabolism in the diabetic liver leads to inadequate removal of lipid peroxides, proved here by elevated lipid peroxidation markers, that finally lead to ferroptosis. This is significantly suppressed by SFN treatment, which improves GSH metabolism by Nrf2 activation, that is, increases GSH amount and GPX4 protein expression, thereby improving the ability to remove lipid peroxides.

Finally, the advantageous effects of SFN-induced Nrf2 activation demonstrated at the molecular level were reflected in corresponding improvement in tissue morphology and biochemical parameters clearly confirming amelioration of liver function by SFN. Namely, SFN improved glucose and lipid metabolism, as shown by the increase in glycogen deposition in the liver, which is normally diminished in diabetes, normalization of glycemia and insulin level, while serum triglycerides level were decreased, indicating reduced triglyceride production in the liver of DM mice treated with SFN.<sup>68</sup> This is in line with the described beneficial effects of SFN in diabetes, which act positively on glucose metabolism by regulating the production and uptake of glucose. In fact, SFN has been shown to reduce hepatic glucose production in patients with T2D,<sup>19</sup> as well as in mouse hepatocytes by controlling Nrf2-signaling axis.<sup>19</sup> On the other hand, by increasing insulin secretion<sup>23</sup> and reducing insulin resistance in diabetic condition, SFN ameliorates glucose uptake with consequent reduction of hyperglycemia.<sup>25</sup> Liver injury is indicated by elevated ALT and AST in the serum,<sup>69</sup> as well as by the appearance of fibrosis in the liver tissue, which represents a sort of scar tissue at the site of hepatocyte death.<sup>70,71</sup> The observed effect of SFN on the normalization of ALT and AST, as well as the protective effect on diabetes-induced liver matrix fibrosis, both suggest that SFN suppresses diabetic liver damage, which is in agreement with the previously described protective effects of SFN on various liver injuries.<sup>31,72,73</sup>

Taken together, our results demonstrate a potent effect of SFN in inhibiting ferroptotic death of hepatocytes under diabetic conditions *in vivo*, thereby alleviating liver injury. To date, the anti-ferroptotic effect of SFN

has been demonstrated in only a few studies, namely in the prevention of busulfan-induced oligospermia in mice,<sup>74</sup> in a diabetic model of cardiomyopathy,<sup>15</sup> and in myocardial ischemia–reperfusion injury in diabetic rats.<sup>17</sup> In the liver, the anti-ferroptotic effect of SFN has recently been demonstrated in acute liver injury<sup>28</sup> and nonalcoholic fatty liver disease<sup>29</sup> models. However, to our knowledge, this is the first study to demonstrate the protective role of SFN against ferroptosis in the liver of diabetic mice.

In conclusion, the hepatoprotective effects of SFN in diabetes noted here are achieved by inhibiting ferroptosis via activation of Nrf2 signaling pathways in hepatocytes, particularly those directed at regulating iron and GSH metabolism. In addition, the study sheds new light on the anti-ferroptotic effect of SFN by attenuating ferritinophagy. The data also imply that the anti-ferroptotic potential of SFN would be worthy of more extensive investigation particularly because a single experimental model was used in the present study, potentially limiting our results to a broader context. Using spontaneously developing autoimmune diabetic mice as well as transgenic and knockout mouse models that mimic the diversity observed in human diabetic patients, the therapeutic effects of SFN on the pathological progression of the disease could be confirmed and translation into clinical practice would be possible. Our efforts along these lines are in progress.

## 4 | MATERIALS AND METHODS

### 4.1 | Experimental procedure

Male C57BL/6 mice, 8–10 weeks old, were housed in the animal facility of the Institute for Biological Research “Sinisa Stankovic” under the standard dark–light cycle and received commercial food and fresh water *ad libitum*. All experimental procedures were approved by the Ethics Committee of the Institute for Biological Research “Sinisa Stankovic” (App. No. 323-37-11487/2021-05) according to Directive 2010/63/EU. The animals were divided into four groups ( $n = 8$ ): control (Ctrl), diabetic (DM), diabetic treated with SFN (DM + SFN), and non-diabetic SFN-treated (SFN). Diabetes was induced by multiple low doses of streptozotocin (STZ, 40 mg/kg body mass; S0130, Sigma-Aldrich, St. Louis, MI, USA) injected intraperitoneally (i.p.) for 5 consecutive days (Days 1–5) as previously described.<sup>10</sup> SFN (2.5 mg/kg; Abcam, Cambridge, UK), was first dissolved in dimethyl sulfoxide (DMSO, D8418, Sigma-Aldrich, St. Louis, MI, USA) diluted in phosphate-buffered saline (PBS), and given i.p., once daily from Days 1 to 42. To avoid possible

interference, the injections of STZ and SFN were administered 3 h apart. The control group received the diluents in the same amount. Once a week, blood glucose levels were measured using a drop of blood from the tail vein of the mice with an Accu-Check glucometer with disposable strips (Accu-Check Performa, Roche Diabetes Care GmbH, Mannheim, Germany). Twenty-four hours after the last SFN administration, the animals were euthanized by cervical dislocation between 9:00 and 9:30 a.m. Blood and liver samples were collected and routinely processed for biochemical, microscopic, immunoblot, and spectrophotometric analysis.

## 4.2 | Biochemical serum analysis

After blood isolation, serum was prepared and stored at  $-80^{\circ}\text{C}$  until further analysis. Kinetic assays of alanine aminotransferase (ALT) and aspartate aminotransferase (AST) activity, as well as colorimetric measurement of triglycerides (TG) level in serum were determined spectrophotometrically (Shimadzu UV-160 spectrophotometer, Kyoto, Japan) using Bioanalytica kits (ALT-250, AST-250, and TRG-210, respectively, Bioanalytica, Belgrade, Serbia). Serum insulin level was measured by radioimmunoassay (INEP, Belgrade, Serbia).

## 4.3 | Microscopic examination of liver

Immediately after isolation, the pieces of liver tissue were fixed overnight in 10% formaldehyde at  $+4^{\circ}\text{C}$ . After 24 h, the tissue was dehydrated with graded ethanol, and then routinely processed for embedding in paraffin blocks. The tissue was cut into  $5\text{-}\mu\text{m}$ -thin sections that were deparaffinized and rehydrated prior to staining. In case of all histological and histochemical staining, slides from three animals per group were examined with a DMLB microscope (Leica Microsystems, Wetzlar, Germany), while for fluorescence staining, samples were analyzed with an SP5 confocal microscope (Leica Microsystems).

### 4.3.1 | Liver fibrosis detection: Heidenhain's AZAN trichrome staining

Rehydrated sections were incubated in filtrated 1% azo-carmin B at  $56^{\circ}\text{C}$  for 10 min. After rinsing in distilled water, staining was shortly differentiated in freshly prepared 1% aniline alcohol, prior to 1 h incubation in 5% phosphomolybdic acid which was followed by the staining in the mixture of 0.2% aniline blue and 0.7% orange G dissolved in 2.7% acetic acid. After thorough washing,

routine dehydration and mounting in dibutyl phthalate polystyrene xylene (DPX) (Sigma-Aldrich, St. Louis, MI, USA) were performed. Fibrosis, that is, accumulation of collagen fibers was stained blue.

### 4.3.2 | Glycogen detection: Periodic acid Schiff (PAS) staining

The rehydrated sections were oxidized in 1% periodic acid for 5 min, washed in distilled water, and then incubated in Schiff's reagent for 15 min. After thorough washing in water, counterstaining with Harris hematoxylin was performed, followed by differentiation in acetic alcohol (1% HCl in 70% ethanol). Sections were washed, dehydrated and mounted in DPX. Glycogen depots and some basement membranes were stained red/magenta and nuclei were stained blue.

### 4.3.3 | Lipofuscin detection: Sudan Black B staining

To detect the accumulation of lipofuscin in liver tissue, a drop of filtrated 0.7% Sudan Black B dissolved in 70% ethanol was applied to a clean glass slide and covered with a slide containing rehydrated liver section. After 30 min, slides were washed in 50% ethanol and distilled water, counterstained in nuclear fast red (NFR) stain, washed, and mounted in Biomount Aqua mounting medium (BioGnost, Croatia). Lipofuscin granules were detected as black/brown particles within the magenta-stained cytoplasm and nuclei.

### 4.3.4 | Iron detection: Pearl's staining

To detect the presence of intracellular nonheme iron ( $\text{Fe}^{3+}$ ) accumulation in the liver, rehydrated sections were incubated in a 2% potassium ferrocyanide solution for 1 h. After washing in distilled water, sections were counterstained with NFR for 2 min, washed, dehydrated, and routinely mounted in DPX. Lung sections were used as a positive control. The cells with blue particles within were considered as iron-containing.

### 4.3.5 | Immunohistochemical staining

Prior to immunohistochemical detection, the step of antigen retrieval was performed by boiling the rehydrated liver sections in citrate buffer (pH 6.0) for about 2 min in the microwave oven. After cooling, the activity of

endogenous peroxidases was inhibited by incubating the slides in 3% H<sub>2</sub>O<sub>2</sub> dissolved in methanol. To block nonspecific antigen binding, 10% normal goat serum (NGS; 1:10, X0907, Dako, Carpinteria, CA, USA) was used (1 h at room temperature). Then, sections were incubated overnight at +4°C with the following primary rabbit antibodies anti-Nrf2 (ab31163; 1:100), anti-4-hydroxy-2-nonenal (4-HNE, ab46545; 1:500) or with the primary mouse antibody anti-divalent metal transporter 1 (DMT1, ab55735; 4 µg/mL), all purchased from Abcam (Cambridge, UK). After rinsing in PBS, incubation with a matching secondary goat anti-rabbit antibody (ab97051, 1:1000, Abcam) and goat anti-mouse antibody (ab97019, 1:200, Abcam) for 1 h at room temperature was performed. DAB chromogen solution (K 3408, Dako liquid DAB + substrate chromogen substrate system) was used to visualize the immunohistochemical reaction. After counterstaining with hematoxylin, the slides were mounted with DPX. To calculate the percentage of Nrf2-positive nuclei of centrilobular hepatocytes, 10 micrographs of centrilobular regions per animal were analyzed at ×40 objective magnification using Image J software (National Institutes of Health, Bethesda, MD, USA). Three animals per group were examined, and the percentage of positive nuclei of hepatocytes was calculated as the ratio of Nrf2-positive nuclei to total nuclei of hepatocytes in the first three rows surrounding the central veins of lobules. To quantify 4-HNE tissue immunopositivity, 20 fields from ×40 magnification micrographs were measured using ImageJ Colour Deconvolution plug-in (H-DAB setup), in order to obtain images with DAB signal only. These were used to determine mean gray scale value of tissue immunopositivity per group. Arbitrary values were calculated as 1000/gray scale level to obtain a direct proportionality between the signal intensity and the measured values (from 0 to 255). The negative control for all immunohistochemistry stainings can be found in Figure S1.

#### 4.3.6 | Immunofluorescence staining

Double immunofluorescence detection of ferritin heavy chain (FTH1) and microtubule-associated protein 1A/1B-light chain 3 (LC3) was performed on rehydrated samples after routine antigen retrieval in citrate buffer (as described in Section 2.3.5) and blocking of nonspecific binding in 10% NGS in bovine serum albumin (BSA) (1 h at room temperature). The mixture of primary antibodies anti-FTH1 (sc-376594; 1:200, Santa Cruz Biotechnology, Dallas, TX, USA) and anti-LC3 (L7543, 1:200, Sigma-Aldrich, St. Louis, MI, USA) was diluted in 5% NGS in 0.1% Triton-X in TBS (TBS-Triton) and applied to the sections overnight at +4°C. After extensive washing in TBS-Triton, the mixture of the appropriate secondary

antibodies (Alexa Fluor 488, goat anti-rabbit, ab150077 and Alexa Fluor 594, goat anti-mouse, ab150116; both from Abcam) was applied for 1 h at room temperature, in the dark. After washing in TBS-Triton and TBS, nuclear counterstaining with Sytox Orange (1:1000 in TBS; Thermo Fisher Scientific, Carlsbad, CA, USA) was performed for 5 min, and sections were washed and mounted in Fluoromount G mounting medium (Thermo Fisher Scientific). During microscopic examination, in order to prevent “bleed through” between detection channels and to better distinguish signals, simultaneous scanning was performed and contrast pseudo colors were assigned to detect signals—green for FTH1, red for LC3, and blue for Sytox Orange. To quantify the intensity of immunopositivity of both proteins inside hepatocytes, approximately 20 randomly selected cells per animal were circled in the software LAS AF (Leica Microsystems) and the mean gray scale values per group were presented. The same software was used for the analysis of FTH1 and LC3 signal colocalization inside hepatocytes. Cells were randomly selected and results were presented as mean Pearson's coefficient per group.

#### 4.4 | Determination of GSH content and activity of antioxidative enzymes in the liver

For determination of the antioxidative enzyme activities, a piece of dissected liver from each animal ( $n = 8$  per group) was subjected to mechanical lysis in the sucrose buffer (0.25 M sucrose, 1 mM EDTA, and 50 mM Tris-HCl pH 7.4). To determine the GSH content, part of the homogenate was deproteinated with 10% sulfosalicylic acid and centrifuged at 5000 rpm/5 min/+4°C. Total GSH was measured from the supernatant by the enzyme-recycling assay of Griffith<sup>75</sup> and expressed in nmol GSH min<sup>-1</sup> g<sup>-1</sup> tissue. The rest of the homogenates were centrifuged at 37,500 rpm/1.30 h/+4°C. Supernatant was used to determine the activity of total superoxide dismutase (SOD) and manganese-superoxide dismutase (MnSOD). The activity of SOD was determined according to the method described by Misra and Fridovich<sup>76</sup> and expressed in units mg<sup>-1</sup> of proteins. SOD units were defined as the amount of enzyme that inhibits the autoxidation of epinephrine under the appropriate reaction conditions.

#### 4.5 | SDS-polyacrylamide gel electrophoresis and Western blot analysis

To examine protein expression in the liver, a tissue homogenate was prepared in sucrose buffer (0.25 M

sucrose, 1 mM EDTA, and 50 mM Tris–HCl pH 7.4) containing protease and phosphatase inhibitors (Protease Inhibitor MixG, #39101, Serva Electrophoresis, Heidelberg, Germany). The prepared homogenates were centrifuged at 37,500 rpm/1.30 h/+4°C. Subsequently, the supernatant was used to determine protein concentration according to a method of Lowry et al.<sup>77</sup> Prior to western blotting, eight homogenates from each group were pooled by three, thus obtaining three samples per group, where the first and second samples were made by coupling homogenates of three animals each and the third one by pooling the two remaining animals. Five or 10 µg of protein from the total cell lysate was loaded onto a 10% or 12% gel and then separated by electrophoresis. The separated proteins were transferred to polyvinylidene fluoride (PVDF) membranes (10600023, Amersham Hybond P 0.45 PVDF, GE Healthcare Life Sciences, Sunderland, UK) overnight at +4°C. Prior to immunoblotting, all membranes were incubated in 5% BSA dissolved in TBST (0.2% Tween 20, 50 mM Tris–HCl pH 7.6, 150 mM NaCl). Primary rabbit antibodies: β-actin (1:2000; ab8227), anti-catalase (CAT, 1:8000; ab1877), anti-cystathionine β-synthase (CBS, 1:4000; ab96252), anti-cystathionase (CTH, 1:1000; ab125210), anti-ferroportin 1 (FPN1, 1:1000; ab78066), anti-glutamate-cysteine ligase (GCLC, 1:5000; ab190685), anti-glutamate-cysteine ligase modifier subunit (GCLM, 1:1000; ab81445), anti-GPX4 (1:1000; ab125066), anti-glutathione reductase (GR, 1:8000; ab16801), anti-Nrf2 (1:1000; ab137550), and anti-thioredoxin reductase (TrxR, 1:10,000; ab124954) all purchased from Abcam; anti-FTH1 (1:1000; CST#3998), anti-phospho-acetyl-CoA carboxylase (pACC, 1:1000; CST#3661) and anti-xCT (1:1000; CST#12691) from Cell Signaling Technology (Danvers, MA, USA); as well as anti-glutathione synthetase (GSS, 1:5000; PA5-37307) and anti-phospho-Nrf2 (pNrf2, 1:1000; PA5-67520) purchased from Thermo Fisher Scientific, Carlsbad, CA, USA, and finally, primary mouse anti-β-actin (1:2000; ab8226) purchased from Abcam were incubated overnight, at +4°C or 1–2 h at room temperature, with constant gentle rocking. Then, membranes were washed six times for 5 min in TBST, after which HRP-conjugated anti-rabbit IgG appropriate secondary antibodies (ab205718 or ab6721, both from Abcam), or anti-mouse (1:1000; CST#7076) from Cell Signaling Technology were probed for 1 h at room temperature. A chemiluminescence reaction with protein bands was obtained using Luminol and 30% H<sub>2</sub>O<sub>2</sub>, after which the bands were visualized using an iBright CL1500 Imaging System (Thermo Fisher Scientific). Membranes were re-probed according to the stripping protocol which includes fast rocking of membranes in 200 mM NaOH (2 × 5 min), after which the membranes were incubated in 5% BSA and re-probed with the appropriate primary antibodies. To quantify protein expression, densitometric analysis of protein

bands was performed using ImageJ software, version 1.8.0\_172. The ratio of the pixel number of target protein band and loading control was averaged from three different experiments and presented relative to the control group, which was standardized as 100%.

#### 4.6 | Statistical analyses of data

Data were statistically analyzed in GraphPad Prism software, version 8.0.2 (San Diego, CA, USA). To determine whether the analyzed parameter has a normal distribution, the Kolmogorov–Smirnov test was applied. One-way analysis of variance (one-way ANOVA) was performed in case of parametric distribution, and Kruskal–Wallis test in case of nonparametric distribution. If the result of the *F* test indicated a difference between the groups, a Tukey/Dunn's post hoc test was performed to determine whether the means of each group is statistically significant. For statistical analysis of the difference between the groups in terms of glycemia and incidence of diabetes through the time, a two-way analysis of variance (two-way ANOVA) was performed, followed by Tukey post hoc test for serum glucose level and Sidak post hoc test for diabetes incidence. Data are presented as the mean ± standard deviation (SD) or standard error of the mean (SEM). If the *p* < 0.05, null hypothesis was rejected and changes of variables were considered as statistically significant.

#### AUTHOR CONTRIBUTIONS

*Conceptualization:* V.O., A.S., and I.G. *Methodology:* V.O., A.S., N.S., M.M., and I.G. *Investigation:* N.S., V.O., M.M., A.S., K.V., I.G., A.G., M.V., and V.M. *Formal analysis:* N.S., V.O., A.S., M.M., K.V., and I.G. *Writing—original draft preparation:* N.S., V.O., and A.S. *Writing—review and editing:* N.S., V.O., A.S., I.G., M.M., and K.V. *Supervision:* V.O. All authors have read and agreed to the published version of the manuscript.

#### FUNDING INFORMATION

This work was supported by The Ministry of Science, Technological Development and Innovation of the Republic of Serbia (contract no. 451-03-47/2023-01/200007) and the Science Fund of the Republic of Serbia (Serbian Science and Diaspora Collaboration Program: Knowledge Exchange Vouchers, #grant no. 6525651, ferroptosis in the b-cells death: possible strategy for diabetes treatment, acronym: BetFeSis).

#### CONFLICT OF INTEREST STATEMENT

The authors declare that the research was conducted in the absence of any commercial or financial relationships that could be construed as a potential conflict of interest.

## DATA AVAILABILITY STATEMENT

Data are available on request.

## ORCID

Nevena Savic  <https://orcid.org/0000-0002-8282-1050>

Ksenija Velickovic  <https://orcid.org/0000-0002-4373-5483>

Vesna Otasevic  <https://orcid.org/0000-0001-8660-8284>

## REFERENCES

- Forbes JM, Cooper ME. Mechanisms of diabetic complications. *Physiol Rev.* 2013;93:137–88. <https://doi.org/10.1152/physrev.00045.2011>
- Mohamed J, Nazratun Nafizah AH, Zariyantey AH, Budin SB. Mechanisms of diabetes-induced liver damage: the role of oxidative stress and inflammation. *Sultan Qaboos Univ Med J.* 2016;16:e132–41. <https://doi.org/10.18295/squmj.2016.16.02.002>
- Afrin R, Arumugam S, Soetikno V, Thandavarayan RA, Pitchaimani V, Karuppagounder V, et al. Curcumin ameliorates streptozotocin-induced liver damage through modulation of endoplasmic reticulum stress-mediated apoptosis in diabetic rats. *Free Radic Res.* 2015;49:279–89. <https://doi.org/10.3109/10715762.2014.999674>
- Rodriguez V, Plavnik L, Tolosa de Talamoni N. Naringin attenuates liver damage in streptozotocin-induced diabetic rats. *Biomed Pharmacother.* 2018;105:95–102. <https://doi.org/10.1016/j.biopha.2018.05.120>
- Liang W, Zhang D, Kang J, Meng X, Yang J, Yang L, et al. Protective effects of rutin on liver injury in type 2 diabetic db/db mice. *Biomed Pharmacother.* 2018;107:721–8. <https://doi.org/10.1016/j.biopha.2018.08.046>
- Grigorov I, Bogojevic D, Jovanovic S, Petrovic A, Ivanovic-Matic S, Zolotarevski L, et al. Hepatoprotective effects of melatonin against pronecrotic cellular events in streptozotocin-induced diabetic rats. *J Physiol Biochem.* 2014;70:441–50. <https://doi.org/10.1007/s13105-014-0322-7>
- Loria P, Lonardo A, Anania F. Liver and diabetes. A vicious circle. *Hepatol Res.* 2013;43:51–64. <https://doi.org/10.1111/j.1872-034X.2012.01031.x>
- Petrovic A, Bogojevic D, Korac A, Golic I, Jovanovic-Stojanov S, Martinović V, et al. Oxidative stress-dependent contribution of HMGB1 to the interplay between apoptosis and autophagy in diabetic rat liver. *J Physiol Biochem.* 2017;73:511–21. <https://doi.org/10.1007/s13105-017-0574-0>
- Shi C, Wang Q, Rao Z, Shi Y, Wei S, Wang H, et al. Diabetes induces hepatocyte pyroptosis by promoting oxidative stress-mediated NLRP3 inflammasome activation during liver ischaemia and reperfusion injury. *Ann Transl Med.* 2020;8:739. <https://doi.org/10.21037/atm-20-1839>
- Stancic A, Velickovic K, Markelic M, Grigorov I, Saksida T, Savic N, et al. Involvement of ferroptosis in diabetes-induced liver pathology. *Int J Mol Sci.* 2022;23:9309. <https://doi.org/10.3390/ijms23169309>
- Dixon SJ, Lemberg KM, Lamprecht MR, Skouta R, Zaitsev EM, Gleason CE, et al. Ferroptosis: an iron-dependent form of non-apoptotic cell death. *Cell.* 2012;149:1060–72. <https://doi.org/10.1016/j.cell.2012.03.042>
- Dodson M, Castro-Portuguez R, Zhang DD. NRF2 plays a critical role in mitigating lipid peroxidation and ferroptosis. *Redox Biol.* 2019;23:101107. <https://doi.org/10.1016/j.redox.2019.101107>
- Ma H, Wang X, Zhang W, Li H, Zhao W, Sun J, et al. Melatonin suppresses ferroptosis induced by high glucose via activation of the Nrf2/HO-1 signaling pathway in type 2 diabetic osteoporosis. *Oxid Med Cell Longev.* 2020;2020:9067610. <https://doi.org/10.1155/2020/9067610>
- Li S, Zheng L, Zhang J, Liu X, Wu Z. Inhibition of ferroptosis by up-regulating Nrf2 delayed the progression of diabetic nephropathy. *Free Radic Biol Med.* 2021;162:435–49. <https://doi.org/10.1016/j.freeradbiomed.2020.10.323>
- Wang X, Chen X, Zhou W, Men H, Bao T, Sun Y, et al. Ferroptosis is essential for diabetic cardiomyopathy and is prevented by sulforaphane via AMPK/NRF2 pathways. *Acta Pharm Sin B.* 2022;12:708–22. <https://doi.org/10.1016/j.apsb.2021.10.005>
- Wei Z, Shaohuan Q, Pinfang K, Chao S. Curcumin attenuates ferroptosis-induced myocardial injury in diabetic cardiomyopathy through the Nrf2 pathway. *Cardiovasc Ther.* 2022;2022:3159717. <https://doi.org/10.1155/2022/3159717>
- Tian H, Xiong Y, Zhang Y, Leng Y, Tao J, Li L, et al. Activation of NRF2/FPN1 pathway attenuates myocardial ischemia-reperfusion injury in diabetic rats by regulating iron homeostasis and ferroptosis. *Cell Stress Chaperones.* 2021;27:149–64. <https://doi.org/10.1007/s12192-022-01257-1>
- Stancic A, Saksida T, Markelic M, Vucetic M, Grigorov I, Martinovic V, et al. Ferroptosis as a novel determinant of beta-cell death in diabetic conditions. *Oxid Med Cell Longev.* 2022;2022:3873420. <https://doi.org/10.1155/2022/3873420>
- Kim M, Lee JY. Beneficial effects of sulforaphane on diabetes and its complications via both Nrf2-dependent and independent mechanisms. *Food Suppl Biomater Health.* 2023;3:e6.
- Houghton CA, Fassett RG, Coombes JS. Sulforaphane and other nutrigenomic Nrf2 activators: can the Clinician's expectation be matched by the reality? *Oxid Med Cell Longev.* 2016;2016:7857186. <https://doi.org/10.1155/2016/7857186>
- Abukhabta S, Khalil Ghawi S, Karatzas KA, Charalampopoulos D, McDougall G, Allwood JW, et al. Sulforaphane-enriched extracts from glucoraphanin-rich broccoli exert antimicrobial activity against gut pathogens in vitro and innovative cooking methods increase in vivo intestinal delivery of sulforaphane. *Eur J Nutr.* 2021;60:1263–76. <https://doi.org/10.1007/s00394-020-02322-0>
- Zheng W, Li X, Zhang T, Wang J. Biological mechanisms and clinical efficacy of sulforaphane for mental disorders. *Gen Psychiatr.* 2022;35:e100700. <https://doi.org/10.1136/gpsych-2021-100700>
- Elbarbry FA, Elrody N. Potential health benefits of sulforaphane: a review of the experimental, clinical and epidemiological evidences and underlying mechanisms. *J Med Plants Res.* 2011;5:473–84.
- Mohammed A, Mohammed HA. Beneficial role of broccoli and its active ingredient, sulforaphane in the treatment of diabetes. *Phytomed Plus.* 2023;3:100431. <https://doi.org/10.1016/j.phyplu.2023.100431>
- Zhang Y, Wu Q, Liu J, Zhang Z, Ma X, Zhang Y, et al. Sulforaphane alleviates high fat diet-induced insulin resistance via





- AMPK/Nrf2/GPx4 axis. *Biomed Pharmacother.* 2022;152:113273. <https://doi.org/10.1016/j.biopha.2022.113273>
26. Wang F, Huang X, Sun Y, Li Z, Sun R, Zhao T, et al. Sulforaphane regulates the proliferation of leukemia stem-like cells via Sonic Hedgehog signaling pathway. *Eur J Pharmacol.* 2022; 919:174824. <https://doi.org/10.1016/j.ejphar.2022.174824>
  27. Isaacson RH, Beier JI, Khoo NK, Freeman BA, Freyberg Z, Arteel GE. Olanzapine-induced liver injury in mice: aggravation by high-fat diet and protection with sulforaphane. *J Nutr Biochem.* 2020;81:108399. <https://doi.org/10.1016/j.jnutbio.2020.108399>
  28. Liu J, Huang C, Liu J, Meng C, Gu Q, du X, et al. Nrf2 and its dependent autophagy activation cooperatively counteract ferroptosis to alleviate acute liver injury. *Pharmacol Res.* 2023; 187:106563. <https://doi.org/10.1016/j.phrs.2022.106563>
  29. Liu P, Anandhan A, Chen J, Shakya A, Dodson M, Ooi A, et al. Decreased autophagosome biogenesis, reduced NRF2, and enhanced ferroptotic cell death are underlying molecular mechanisms of non-alcoholic fatty liver disease. *Redox Biol.* 2023;59:102570. <https://doi.org/10.1016/j.redox.2022.102570>
  30. Briones-Herrera A, Eugenio-Perez D, Reyes-Ocampo JG, Rivera-Mancia S, Pedraza-Chaverri J. New highlights on the health-improving effects of sulforaphane. *Food Funct.* 2018;9: 2589–606. <https://doi.org/10.1039/c8fo00018b>
  31. Zhao HD, Zhang F, Shen G, Li YB, Li YH, Jing HR, et al. Sulforaphane protects liver injury induced by intestinal ischemia reperfusion through the Nrf2-ARE pathway. *World J Gastroenterol.* 2010;16:3002–10. <https://doi.org/10.3748/wjg.v16.i24.3002>
  32. Huang Y, Li W, Su ZY, Kong AN. The complexity of the Nrf2 pathway: beyond the antioxidant response. *J Nutr Biochem.* 2015;26:1401–13. <https://doi.org/10.1016/j.jnutbio.2015.08.001>
  33. Su X, Wang S, Zhang H, Yang G, Bai Y, Liu P, et al. Sulforaphane prevents angiotensin II-induced cardiomyopathy by activation of Nrf2 through epigenetic modification. *J Cell Mol Med.* 2021;25:4408–19. <https://doi.org/10.1111/jcmm.16504>
  34. Velmurugan GV, Sundaresan NR, Gupta MP, White C. Defective Nrf2-dependent redox signalling contributes to microvascular dysfunction in type 2 diabetes. *Cardiovasc Res.* 2013;100: 143–50. <https://doi.org/10.1093/cvr/cvt125>
  35. Bai Y, Cui W, Xin Y, Miao X, Barati MT, Zhang C, et al. Prevention by sulforaphane of diabetic cardiomyopathy is associated with up-regulation of Nrf2 expression and transcription activation. *J Mol Cell Cardiol.* 2013;57:82–95. <https://doi.org/10.1016/j.yjmcc.2013.01.008>
  36. Ruhee RT, Suzuki K. The integrative role of sulforaphane in preventing inflammation, oxidative stress and fatigue: a review of a potential protective phytochemical. *Antioxidants (Basel).* 2020;9:521. <https://doi.org/10.3390/antiox9060521>
  37. Tang D, Kroemer G. Ferroptosis. *Curr Biol.* 2020;30:R1292–7. <https://doi.org/10.1016/j.cub.2020.09.068>
  38. Zhou R, Lin J, Wu D. Sulforaphane induces Nrf2 and protects against CYP2E1-dependent binge alcohol-induced liver steatosis. *Biochim Biophys Acta.* 2014;1840:209–18. <https://doi.org/10.1016/j.bbagen.2013.09.018>
  39. Zhang Z, Wang S, Zhou S, Yan X, Wang Y, Chen J, et al. Sulforaphane prevents the development of cardiomyopathy in type 2 diabetic mice probably by reversing oxidative stress-induced inhibition of LKB1/AMPK pathway. *J Mol Cell Cardiol.* 2014; 77:42–52. <https://doi.org/10.1016/j.yjmcc.2014.09.022>
  40. Chang YW, Jang JY, Kim YH, Kim JW, Shim JJ. The effects of broccoli sprout extract containing sulforaphane on lipid peroxidation and *Helicobacter pylori* infection in the gastric mucosa. *Gut Liver.* 2015;9:486–93. <https://doi.org/10.5009/gnl14040>
  41. Cho BO, Ryu HW, Jin CH, Choi DS, Kang SY, Kim DS, et al. Blackberry extract attenuates oxidative stress through up-regulation of Nrf2-dependent antioxidant enzymes in carbon tetrachloride-treated rats. *J Agric Food Chem.* 2011;59:11442–8. <https://doi.org/10.1021/jf2021804>
  42. Huang XS, Chen HP, Yu HH, Yan YF, Liao ZP, Huang QR. Nrf2-dependent upregulation of antioxidative enzymes: a novel pathway for hypoxic preconditioning-mediated delayed cardioprotection. *Mol Cell Biochem.* 2014;385:33–41. <https://doi.org/10.1007/s11010-013-1812-6>
  43. Delgobo M, Goncalves RM, Delazeri MA, Falchetti M, Zandona A, Nascimento das Neves R, et al. Thioredoxin reductase-1 levels are associated with NRF2 pathway activation and tumor recurrence in non-small cell lung cancer. *Free Radic Biol Med.* 2021;177:58–71. <https://doi.org/10.1016/j.freeradbiomed.2021.10.020>
  44. Vnukov VV, Gutsenko OI, Milyutina NP, Kornienko IV, Ananyan AA, Plotnikov AA, et al. SkQ1 regulates expression of Nrf2, ARE-controlled genes encoding antioxidant enzymes, and their activity in cerebral cortex under oxidative stress. *Biochemistry (Mosc).* 2017;82:942–52. <https://doi.org/10.1134/S0006297917080090>
  45. Ahmadi Z, Ashrafzadeh M. Melatonin as a potential modulator of Nrf2. *Fundam Clin Pharmacol.* 2020;34:11–9. <https://doi.org/10.1111/fcp.12498>
  46. Qader M, Xu J, Yang Y, Liu Y, Cao S. Natural Nrf2 activators from juices, wines, coffee, and cocoa. *Beverages.* 2020;6:68.
  47. Zhang J, Svehlíková V, Bao Y, Howie AF, Beckett GJ, Williamson G. Synergy between sulforaphane and selenium in the induction of thioredoxin reductase 1 requires both transcriptional and translational modulation. *Carcinogenesis.* 2003; 24:497–503. <https://doi.org/10.1093/carcin/24.3.497>
  48. Kasai S, Mimura J, Ozaki T, Itoh K. Emerging regulatory role of Nrf2 in iron, heme, and hemoglobin metabolism in physiology and disease. *Front Vet Sci.* 2018;5:242. <https://doi.org/10.3389/fvets.2018.00242>
  49. Stockwell BR, Friedmann Angeli JP, Bayir H, Bush AI, Conrad M, Dixon SJ, et al. Ferroptosis: a regulated cell death nexus linking metabolism, redox biology, and disease. *Cell.* 2017;171:273–85. <https://doi.org/10.1016/j.cell.2017.09.021>
  50. Kerins MJ, Ooi A. The roles of NRF2 in modulating cellular iron homeostasis. *Antioxid Redox Signal.* 2018;29:1756–73. <https://doi.org/10.1089/ars.2017.7176>
  51. Chen X, Yu C, Kang R, Tang D. Iron metabolism in ferroptosis. *Front Cell Dev Biol.* 2020;8:590226. <https://doi.org/10.3389/fcell.2020.590226>
  52. Zhao Y, Zhang R, Wang Z, Chen Z, Wang G, Guan S, et al. Melatonin prevents against ethanol-induced liver injury by mitigating ferroptosis via targeting brain and muscle ARNT-like 1 in mice liver and HepG2 cells. *J Agric Food Chem.* 2022;70: 12953–67. <https://doi.org/10.1021/acs.jafc.2c04337>
  53. Saito Y, Yako T, Otsu W, Nakamura S, Inoue Y, Muramatsu A, et al. A triterpenoid Nrf2 activator, RS9, promotes

- LC3-associated phagocytosis of photoreceptor outer segments in a p62-independent manner. *Free Radic Biol Med.* 2020;152:235–47. <https://doi.org/10.1016/j.freeradbiomed.2020.03.012>
54. Frias DP, Gomes RLN, Yoshizaki K, Carvalho-Oliveira R, Matsuda M, Junqueira MS, et al. Nrf2 positively regulates autophagy antioxidant response in human bronchial epithelial cells exposed to diesel exhaust particles. *Sci Rep.* 2020;10:3704. <https://doi.org/10.1038/s41598-020-59930-3>
  55. Latunde-Dada GO. Ferroptosis: role of lipid peroxidation, iron and ferritinophagy. *Biochim Biophys Acta Gen Subj.* 2017;1861:1893–900. <https://doi.org/10.1016/j.bbagen.2017.05.019>
  56. He J, Li Z, Xia P, Shi A, FuChen X, Zhang J, et al. Ferroptosis and ferritinophagy in diabetes complications. *Mol Metab.* 2022;60:101470. <https://doi.org/10.1016/j.molmet.2022.101470>
  57. Li D, Shao R, Wang N, Zhou N, Du K, Shi J, et al. Sulforaphane activates a lysosome-dependent transcriptional program to mitigate oxidative stress. *Autophagy.* 2021;17:872–87. <https://doi.org/10.1080/15548627.2020.1739442>
  58. Greaney AJ, Maier NK, Leppla SH, Moayeri M. Sulforaphane inhibits multiple inflammasomes through an Nrf2-independent mechanism. *J Leukoc Biol.* 2016;99:189–99. <https://doi.org/10.1189/jlb.3A0415-155RR>
  59. Ursini F, Maiorino M. Lipid peroxidation and ferroptosis: the role of GSH and GPx4. *Free Radic Biol Med.* 2020;152:175–85. <https://doi.org/10.1016/j.freeradbiomed.2020.02.027>
  60. Lu SC. Glutathione synthesis. *Biochim Biophys Acta.* 1830;2013:3143–53. <https://doi.org/10.1016/j.bbagen.2012.09.008>
  61. Li Y, Yan H, Xu X, Liu H, Wu C, Zhao L. Erastin/sorafenib induces cisplatin-resistant non-small cell lung cancer cell ferroptosis through inhibition of the Nrf2/xCT pathway. *Oncol Lett.* 2020;19:323–33. <https://doi.org/10.3892/ol.2019.11066>
  62. Sbodio JI, Snyder SH, Paul BD. Regulators of the transsulfuration pathway. *Br J Pharmacol.* 2019;176:583–93. <https://doi.org/10.1111/bph.14446>
  63. Hayes JD, Dinkova-Kostova AT. The Nrf2 regulatory network provides an interface between redox and intermediary metabolism. *Trends Biochem Sci.* 2014;39:199–218. <https://doi.org/10.1016/j.tibs.2014.02.002>
  64. Liu Z, Lv X, Song E, Song Y. Fostered Nrf2 expression antagonizes iron overload and glutathione depletion to promote resistance of neuron-like cells to ferroptosis. *Toxicol Appl Pharmacol.* 2020;407:115241. <https://doi.org/10.1016/j.taap.2020.115241>
  65. Tarozzi A, Morroni F, Merlicco A, Hrelia S, Angeloni C, Cantelli-Forti G, et al. Sulforaphane as an inducer of glutathione prevents oxidative stress-induced cell death in a dopaminergic-like neuroblastoma cell line. *J Neurochem.* 2009;111:1161–71. <https://doi.org/10.1111/j.1471-4159.2009.06394.x>
  66. Ursini F, Bosello Travain V, Cozza G, Miotto G, Roveri A, Toppo S, et al. A white paper on phospholipid hydroperoxide glutathione peroxidase (GPx4) forty years later. *Free Radic Biol Med.* 2022;188:117–33. <https://doi.org/10.1016/j.freeradbiomed.2022.06.227>
  67. Dixon SJ. Ferroptosis: bug or feature? *Immunol Rev.* 2017;277:150–7. <https://doi.org/10.1111/imr.12533>
  68. Akiyama S, Katsumata S, Suzuki K, Ishimi Y, Wu J, Uehara M. Dietary hesperidin exerts hypoglycemic and hypolipidemic effects in streptozotocin-induced marginal type 1 diabetic rats. *J Clin Biochem Nutr.* 2010;46:87–92. <https://doi.org/10.3164/jcbn.09-82>
  69. McGill MR. The past and present of serum aminotransferases and the future of liver injury biomarkers. *EXCLI J.* 2016;15:817–28. <https://doi.org/10.17179/excli2016-800>
  70. Mehal W, Imaeda A. Cell death and fibrogenesis. *Semin Liver Dis.* 2010;30:226–31. <https://doi.org/10.1055/s-0030-1255352>
  71. Eguchi A, Wree A, Feldstein AE. Biomarkers of liver cell death. *J Hepatol.* 2014;60:1063–74. <https://doi.org/10.1016/j.jhep.2013.12.026>
  72. Ishida K, Kaji K, Sato S, Ogawa H, Takagi H, Takaya H, et al. Sulforaphane ameliorates ethanol plus carbon tetrachloride-induced liver fibrosis in mice through the Nrf2-mediated antioxidant response and acetaldehyde metabolism with inhibition of the LPS/TLR4 signaling pathway. *J Nutr Biochem.* 2021;89:108573. <https://doi.org/10.1016/j.jnutbio.2020.108573>
  73. Chi X, Zhang R, Shen N, Jin Y, Alina A, Yang S, et al. Sulforaphane reduces apoptosis and oncosis along with protecting liver injury-induced ischemic reperfusion by activating the Nrf2/ARE pathway. *Hepatol Int.* 2015;9:321–9. <https://doi.org/10.1007/s12072-014-9604-y>
  74. Zhao X, Liu Z, Gao J, Li H, Wang X, Li Y, et al. Inhibition of ferroptosis attenuates busulfan-induced oligospermia in mice. *Toxicology.* 2020;440:152489. <https://doi.org/10.1016/j.tox.2020.152489>
  75. Griffith OW. Determination of glutathione and glutathione disulfide using glutathione reductase and 2-vinylpyridine. *Anal Biochem.* 1980;106:207–12. [https://doi.org/10.1016/0003-2697\(80\)90139-6](https://doi.org/10.1016/0003-2697(80)90139-6)
  76. Misra HP, Fridovich I. The role of superoxide anion in the autoxidation of epinephrine and a simple assay for superoxide dismutase. *J Biol Chem.* 1972;247:3170–5.
  77. Lowry OH, Rosebrough NJ, Farr AL, Randall RJ. Protein measurement with the Folin phenol reagent. *J Biol Chem.* 1951;193:265–75.

## SUPPORTING INFORMATION

Additional supporting information can be found online in the Supporting Information section at the end of this article.

**How to cite this article:** Savic N, Markelic M, Stancic A, Velickovic K, Grigorov I, Vucetic M, et al. Sulforaphane prevents diabetes-induced hepatic ferroptosis by activating Nrf2 signaling axis. *BioFactors.* 2024. <https://doi.org/10.1002/biof.2042>